UCLA
UCLA Previously Published Works

Title

Quantification of the carbon bonding state in amorphous carbon materials: A comparison between EELS and NEXAFS measurements

Permalink

https://escholarship.org/uc/item/8k9050p8

Authors

Mangolini, Filippo
Li, Zixuan
Marcus, Matthew A
et al.

Publication Date

2021-03-01

DOI

10.1016/j.carbon.2020.11.021

Peer reviewed

Quantification of the carbon bonding state in amorphous carbon materials: a comparison between EELS and NEXAFS measurements

Filippo Mangolini[1,2,*], Zixuan Li[1,3], Matthew A. Marcus[4], Reinhard Schneider[5,6], Martin Dienwiebel[6,7]

1. Texas Materials Institute, The University of Texas at Austin, Austin, TX 78712, USA
2. J. Mike Walker Department of Mechanical Engineering, The University of Texas at Austin, Austin, TX 78712, USA
3. Materials Science and Engineering Program, The University of Texas at Austin, Austin, TX 78712, USA
4. Advanced Light Source, Berkeley National Laboratory, Berkeley, CA 94720, USA
5. Karlsruhe Institute for Technology, Institute for Applied Materials, MikroTribologie Centrum µTC, 76128, Karlsruhe, Germany
6. Fraunhofer Institute for Mechanics of Materials IWM, 79108, Freiburg, Germany
7. Laboratory for Electron Microscopy (LEM), Karlsruhe Institute of Technology (KIT), Engesserstrasse 7, 76131 Karlsruhe, Germany

*Corresponding Author: filippo.mangolini@austin.utexas.edu

Keywords: EELS; NEXAFS; STXM; amorphous carbon; DLC.

Abstract

The quantitative determination of the carbon hybridization is critical for establishing processing-structure-properties relationships for carbon-based materials, including amorphous carbon coatings. While several techniques have been employed to characterize the amount of sp^2 and sp^3 carbon in these materials, direct comparisons between analytical results are limited. Here, we compared near edge X-ray absorption fine structure (NEXAFS) spectra of a silicon- and oxygen-containing hydrogenated amorphous carbon (a-C:H:Si:O) coating acquired in synchrotron-based scanning transmission X-ray microscopy (STXM) mode with electron energy loss spectra (EELS) obtained from the same a-C:H:Si:O lamella. While the fractions of sp^2 carbon computed from STXM and EELS spectra are in close agreement, the comparison of NEXAFS spectra acquired in STXM mode with NEXAFS spectra collected in partial electron yield

mode on a flat a-C:H:Si:O surface indicated that the destructive preparation of thin lamellae for STXM analyses induces variations in the structure of a-C:H:Si:O, namely the breakage of carbon-silicon and carbon-hydrogen bonds, a change in ordering of sp^2-bonded carbon, and an increase in the sp^2 carbon fraction. These findings can help scientists in the careful interpretation of spectroscopic results obtained from the analysis of samples made of metastable materials after the destructive preparation of specimens for analytical purposes.

1. **Introduction**

A large number of technical applications, including cutting tools, mechanical seals and biomedical devices, fundamentally rely on carbon-based materials in form of coatings and thin films. Diamond-like carbon (DLC) films, which consist of an amorphous network of carbon atoms with a certain amount of sp^3-type bonds, largely extend the range of applications and are used on automotive components, tools, dies, computer hard disks, and other protective coatings [1]. The fraction of sp^2 and sp^3 bonds of the coating can be tuned during the deposition process of a DLC coating to obtain the desired properties, such as hardness, electrical conductivity, and tribological properties (friction and wear resistance) [1]. Moreover, the sp^3 content has been observed to change during tribological stressing of diamond or DLC films [2–4] and therefore it might strongly influence the lifetime of coated components. For these reasons, it is imperative to experimentally determine the percentage of carbon atoms in a specific hybridization state (sp^2 or sp^3) and be able to obtain quantitative results in an accurate and reproducible fashion.

In order to quantify the percentage of carbon atoms in sp^2 or sp^3 hybridization in DLC coatings, many analytical techniques (either bulk or surface sensitive) have been employed. Early studies employed nuclear magnetic resonance (NMR) (see, *e.g.*, [5, 6]) and electron energy loss spectroscopy (EELS) (see, *e.g.*, [7, 8]) as "gold standard" for the quantification of the carbon bonding in DLCs. However, due to the destructive nature of these techniques, which require the removal of the coating from the substrate in the case of NMR measurements or the preparation of electron-transparent lamellae for

transmission EELS analyses, other techniques such as Raman spectroscopy have gained in popularity to characterize carbon materials. For the quantification of the hybridization state, Tamor and Vassel observed that the ratio of the D to the G peaks (I(D)/I(G)) in visible Raman spectra varied for different types of DLC films [9]. Ferrari and Robertson proposed a relationship between the G-peak position, I(D)/I(G), and the sp^3 fraction based on fits to EELS and NMR data [10]. This relationship is often used nowadays for drawing conclusions about the carbon hybridization in carbon-based materials (see, *e.g.*, [11]). As for surface-sensitive techniques, X-ray photoelectron (XPS) [12–22], Auger electron (AES) [13, 17, 19, 20, 22–24], and near edge X-ray absorption fine structure (NEXAFS) [18, 25–31] spectroscopy have extensively been used. Even though XPS spectroscopy has widely been employed for quantifying the carbon hybridization state through the fit of C 1s signals with two synthetic curves (one assigned to sp^2-bonded carbon and one assigned to sp^3-bonded carbon), the validity of this approach has recently been debated [13, 15]. The quantification of the sp^2 carbon fraction can, however, be obtained using the X-ray induced carbon KLL Auger peak, as the distance between the most negative minimum and the most positive maximum in the first derivative spectrum (called *D*-parameter) linearly varies between 13.7 eV for diamond and 21.2 eV for graphite [13]. Mangolini *et al.* compared the results obtained from NEXAFS, XPS, and Raman spectroscopy and concluded that a good quantitative agreement between these methods can be achieved when carefully selecting the measurement conditions (angle of incidence, integration limits, and corrections for surface contamination) [32]. Similarly Zhang *et al.* [3, 33] observed that the measurement protocol in EELS spectroscopy can critically influence the sp^2 fraction.

Even though NEXAFS spectroscopy has proven powerful for gaining detailed insights the surface termination of carbonaceous materials, the interpretation of NEXAFS data is often challenging owing to the presence of several overlapping absorption features [34, 35]. Recently, Aarva *et al.* effectively combined experimental NEXAFS data with density functional theory calculations to identify and quantify functional groups in the near-surface region of carbonaceous materials [34, 35].

Here, we provide the first, direct comparison between EELS and NEXAFS spectroscopic measurements carried out on the same thin lamella made of an alloyed

version of DLC, namely silicon- and oxygen-containing hydrogenated amorphous carbon (a-C:H:Si:O). The present work provides guidance for the accurate interpretation of quantitative estimates of the fraction of sp^2 carbon obtained on the basis of EELS and NEXAFS analyses of thin lamellae.

2. Experimental

2.1. Materials

Silicon- and oxygen-containing hydrogenated amorphous carbon (a-C:H:Si:O) coatings (thickness: 2 μm) were grown on [100]-oriented n-type silicon wafers using a proprietary plasma-enhanced chemical vapor deposition (PECVD) process developed by Sulzer-Metco Inc. (Amherst, NY, USA). A detailed description of this coating can be found in Ref. [36–38]. Notably, a-C:H:Si:O coatings have moderate electrical conductivity, which allows NEXAFS analysis to be performed without any sample charging issues.

A reference compound was used for NEXAFS and EELS spectroscopic measurements, namely freshly cleaved highly ordered pyrolytic graphite (HOPG, grade 2, SPI Supplies, West Chester, PA, USA).

2.2. Methods
2.2.1. Sample preparation

Thin lamellae of a-C:H:Si:O were prepared in a conventional way, *i.e.*, by face-to-face gluing (two component epoxy-phenolic resin M-Bond 610) two sample pieces, embedding the glued samples in a 3-mm-diameter hollow cylinder, and slicing the cylinder to obtain discs using a precision diamond wire saw of the type WELL 3500, which are later ground, polished, and dimpled (Figure 1). Dimpling of both sides of the discs was performed by a dimple grinder Gatan model 656, starting with a brass wheel and 3 μm diamond paste, continuing with a felt wheel and 1 μm diamond paste, and finally with 0.25 μm diamond paste. To create electron-transparent areas suitable for TEM measurements, further thinning was achieved by ion (Ar$^+$) milling (ion energy: 3

keV) at 5° tilt of the ion guns by means of a precision ion polishing system PIPS model 691 (Gatan). In the final stage, the Ar^+ ion energy was reduced to 1 keV to reduce possible sample damage and ensure that the glue in between the two DLC surfaces was completely removed from the regions of interest. The total Ar^+ ion current amounted to approximately 12 μA, which is a typical value for preparing cross-section TEM specimens from Si-based materials. The creation of a hole in the middle of the sample also allowed for the acquisition of the intensity (I_0) of the incoming X-ray beam during STXM measurements, which is necessary for the computation of the optical density (absorbance).

2.2.2. Electron energy loss spectroscopy (EELS)

For EELS acquisition, a transmission electron microscope (TEM) of the type FEI Titan 80-300 equipped with a Gatan imaging energy filter (GIF) Tridiem model 865 HR was used. The Titan microscope was operated at 80 kV in the microprobe STEM mode to minimize beam damage and carbon contamination. The energy dispersion of the GIF system was set to 0.1 eV/channel and spectrum recording was performed via a 4 mega-pixel Gatan UltraScan 1000 P CCD camera. The time for a single EELS acquisition of the carbon K-edge was 1 s, with a typical electron dose rate of several 10 $e^-/Å^2$ s. In each case, the final carbon energy loss near-edge structure (ELNES) spectrum was obtained by summing up of ~100 single spectra. In addition, low-loss spectra were obtained under a similar setup, except that the electron dose rate and acquisition time were extremely reduced to prevent any beam damage of the scintillator in front of the CCD chip. The convergence angle of the electron probe and the spectrometer acceptance angle were chosen in a way that for HOPG there is no remarkable dependence of the C K-ELNES on the specific sample orientation. This requirement is usually called magic angle condition (MAC) (see, *e.g.*, Hebert *et al.* [39]) and, in detail, for the chosen microprobe illumination it is quite well fulfilled by a choice of a convergence semi-angle of 2.0 mrad and a spectrometer acceptance semi-angle of 3.9 mrad. EELS was done with an energy resolution of approximately 0.7 eV according to the FWHM of the zero-loss peak (ZLP). Besides the thin a-C:H:Si:O lamella under investigation, EELS spectra were also recorded from the HOPG reference under identical experimental conditions. For the

latter, before EELS acquisition the HOPG specimen was first oriented close to a zone axis and channeling effects were then avoided by tilting the specimen by 5-10° away from it. EELS spectra did not change during the combined STEM/EELS experiments, which is an indication for negligible influence of electron-beam irradiation on the sp^2 content as well as negligible deposition of carbonaceous layers on the TEM lamella as a result of the interaction between the incoming electron beam and residual hydrocarbons in the chamber.

To obtain the net C K-ELNES, the measured C K-edge spectra were processed in the standard manner, *i.e.*, the background under the edge was fitted and subtracted by an exponential function of the type $A \cdot E^{-r}$ with A and r as fit parameters, using a pre-edge window of 30 eV width. Subsequently, effects of plural scattering were removed by Fourier-ratio deconvolution with the corresponding low-loss spectra.

2.2.3. Near-edge X-ray absorption fine structure (NEXAFS) spectroscopy

Near edge X-ray absorption fine structure (NEXAFS) spectroscopic analyses were carried out at the Polymer Scanning Transmission X-Ray Microscopy (STXM) beamline (beamline 5.3.2.2) at the Advanced Light Source (ALS), Lawrence Berkeley National Laboratory (Berkeley, CA, USA). A detailed description of the beamline can be found in Ref. [40]. Briefly, the beamline has an energy range between 250 eV and 750 eV and its source is a bending magnet. The photon flux is 1×10^7 photons/second, and the resolving power ($\Delta E/E$) is < 5000. STXMs use Fresnel zone plate optics to achieve a theoretical spot size as low as 30 nm. In the present case, the STXM allowed for imaging a 20 x 4 μm^2 area. The calibration of the monochromator energy was performed using the characteristic π* feature of freshly-cleaved HOPG at 285.5 eV. STXM/NEXAFS data acquisition was performed in image stack mode (images recorded over a sequence of photon energies). Their acquisition of image stacks relied on creating a highly aligned hyperspectral data-set constituted by images acquired over an energy range across a given NEXAFS region. During the collection of image stacks, the sample position was precisely (< 50 nm) controlled by laser interferometry [40]. For NEXAFS data acquired around the carbon K-edge, the acquisition of image stacks was performed between 278 eV and 330 eV with the incidence angle (relative to the plane of the lamellae) of the X-

ray beam equal to 90º for a-C:H:Si:O (note: no variations in the spectra acquired on a-C:H:Si:O were observed upon changing the X-ray incidence angle). The experimental settings used for the acquisition of reference spectra on HOPG are outlined in Section II. The intensity of the transmitted X-ray (I) was converted to absorbance (optical density) by using Beer-Lambert law (*i.e.*, $A = -ln(I/I_0)$), where I_0 is the intensity of the incoming beam as recorded through a region of the field of view where no sample was present. The normalization of the intensity of the transmitted X-ray (I) to the intensity of the incoming beam as recorded through a region of the field of view where no sample was present also allowed for the removal of experimental artefacts, such as the beamline transmission function, carbon contamination on beamline optics, flux monitor contamination, beam stability, and signal offset. The acquired spectra were then normalized to the absorbance in the post-edge region (at 320 eV) so that any changes in spectral intensity only derive from variations in chemical environment and are not dependent on the number of absorbing atoms. Spectra from regions of interest were extracted using aXis 2000 software [41].

3. Results & Discussion

Section I: Comparison between EELS and SXTM/NEXAFS C K-Edge Spectra

A TEM micrograph of two a-C:H:Si:O-coated silicon samples glued upside/down against each other is displayed in Figure 2a. TEM observations were performed in electron-transparent areas around the hole generated in the middle of the sample upon thinning the lamella using Ar^+ ions. The micrographs indicated that a-C:H:Si:O is an amorphous, homogeneous solid solution without any phase separation or crystalline phase, in agreement with previous NMR characterization of the same material [37]. The same region of interest could be located in the scanning transmission X-ray microscope (STXM) at beamline 5.3.2.2. at the Advanced Light Source (Figure 2b). The presence of a hole in the field of view allowed for the acquisition of the intensity of the incoming beam as a function of photon energy (I_0). The intensity of the transmitted X-ray (I) from region of interests on a-C:H:Si:O could thus be converted to absorbance using Beer-Lambert law. Figure 3a shows the STXM/NEXAFS C K-edge spectrum of a-C:H:Si:O

extracted from the area highlighted in Figure 2b together with the NEXAFS carbon K-edge spectrum collected in partial electron yield (PEY) mode from the analysis of the as-deposited coating on silicon (referred to as "flat surface", which did not require any sample preparation. For the acquisition of the NEXAFS C K-edge spectrum of a-C:H:Si:O in PEY mode displayed in Figure 2b, the X-ray incidence angle was 55º, while the entrance grid bias (EGB) voltage of the channeltron detector was set to -225 V with the aim of reducing the number of Auger electrons detected that suffered energy loss while travelling through the specimen. Note: as-grown a-C:H:Si:O films do not exhibit any gradient in the percentage of sp^2 carbon in the near-surface region as indicated by NEXAFS analyses performed in PEY mode at different entrance grid bias (EGB) voltage, *i.e.*, while changing the information depth [42]). Both spectra are pre- and post-edge normalized, thus making any variations in spectral intensity only dependent on the chemical environment. The C K-edge spectra of a-C:H:Si:O in Figure 3a exhibited a peak at 285.0 ± 0.1 eV, which is characteristic of the transition of C 1s electrons to π* orbitals in materials containing disordered carbon-carbon bonds [30, 43]. The intensity of this feature is correlated with the amount of sp^2-hybridized carbon atoms. A broad hump between 288 eV and 320 eV is also detected and due to the transition of C 1s electrons to σ* orbitals [30, 43]. Significant differences could be observed between the spectrum obtained from the flat a-C:H:Si:O surface in PEY mode and the spectrum obtained in STXM transmission mode from the thin lamella (Figure 3b): the characteristic feature of carbon-hydrogen and carbon-silicon bonds in a-C:H:Si:O at, respectively, 287.0 ± 0.1 eV [18, 31, 44] and 288.9 ± 0.1 eV [45] could not be clearly resolved in the latter, thus indicating the breakage of C-H and C-Si bonds during the preparation of the lamella for TEM and STXM measurements. Additionally, the C1s→π* feature in the X-ray absorption spectrum acquired in transmission mode is broader and exhibited a shoulder at high higher photon energies compared to the spectrum acquired in PEY mode. As shown by Grierson *et al.* [29], the broadening of the C1s→π* peak in NEXAFS spectra of tetrahedral amorphous carbon (ta-C) materials is correlated with a broadening of the distribution of bond lengths, whereas the shift to higher energies is indicative for an increase in ordering of sp^2-bonded carbon atoms (the characteristic C1s→π* absorption feature for HOPG is detected at 285.5 eV [38]). These differences indicated that the

preparation of an electron and X-ray transparent lamella also induced a change in local ordering of sp^2 carbon atoms in a-C:H:Si:O.

The STXM C K-edge NEXAFS spectra acquired on a reference HOPG sample (to be used for the quantitative evaluation of the fraction of sp^2 carbon, see Section II) and on a-C:H:Si:O could be compared with the EELS C K-edge spectra (Figure 4). The small feature observed at around 288 eV in the NEXAFS C K-edge spectrum of HOPG together with the small negative slope of the spectrum between 288 and 290 eV suggest a small amount of oxidation of HOPG due to its short exposure to air after being cleaved and before being pumped down. Notably, EELS measurements could be carried out on the same a-C:H:Si:O lamella analyzed by STXM/NEXAFS. Due to the lower energy resolution of EELS compared to synchrotron-based STXM/NEXAFS analyses, the characteristic C1s→π* peak at ~285.0 eV is broader in the former. Similarly, the double-resonance arising from excitonic (sharp feature at 291.8 eV [46]) and band-like contributions (broader signal at 293 eV [46]) are less sharp in EELS spectra due to the lower energy resolution of EELS. Finally, the relative intensity of the C1s→π* and C1s→σ* peaks is significantly different in EELS and STXM/NEXAFS spectra due to dependence of the transition cross-section for a certain spectral component on the experimental conditions (*e.g.*, energy of the impinging radiation).

Section II: Quantification of the Carbon Hybridization State on the Basis of SXTM/NEXAFS and EELS C K-Edge Spectra

While both NEXAFS and EELS spectroscopy have extensively been used for computing the fraction of sp^2 carbon atoms in carbonaceous materials, the methodologies employed for the calculations, although similar, exhibit slight differences. In this section, we briefly review the methodologies reported in the literature and then use them to quantify the hybridization state of carbon in a-C:H:Si:O on the basis of NEXAFS and EELS data acquired on the same lamellae. An extensive review of these methodologies can be found in Ref. [26, 33] together with guidelines for their implementation.

Since dipole transitions dominate NEXAFS spectra for excitation of shells at wavelength much larger than the shell diameter, the methodology developed by Berger *et al.* [7] for the quantitative evaluation of the fraction of carbon in a specific hybridization

state (*i.e.*, sp^2 or sp^3) on the basis of EELS spectra has also been applied to determine the carbon bonding configuration from NEXAFS data [18, 26, 47–51]. The procedure (referred to as "NEXAFS method" in the following) relies on the computation of the ratio of the integrated intensity of the C1s→π* and C1s→σ* peaks for both the sample and a reference specimen:

$$f_{sp^2(NEXAFS)} = \frac{I^{\pi^*}_{sam} I_{ref}(\Delta E)}{I_{sam}(\Delta E) I^{\pi^*}_{ref}}$$

Eq. 1

where $I^{\pi^*}_{sam}$ and $I^{\pi^*}_{ref}$ are, respectively, the areas of the C1s→π* peaks for the sample and reference obtained from fitting this absorption feature with a Gaussian synthetic curve, whereas $I_{sam}(\Delta E)$ and $I_{ref}(\Delta E)$ are the integrated spectrum intensity between two integration limits. Recently, Mangolini *et al.* reviewed this methodology and provided guidance for the conditions (*i.e.*, X-ray beam incident angle) to be used for the acquisition of reference spectra on freshly-cleaved HOPG (100% sp^2-bonded carbon) together with definition of the integration limits to compute the area of the C1s→σ* peak [26]. On the basis of Mangolini *et al.*'s work [26], in the present work HOPG reference spectra were acquired in PEY mode at an X-ray beam incident angle of 40° (relative to the sample surface) to account for the cos^2(Θ) angular dependence of the π* and σ* resonance intensity as well as the X-ray polarization factor (Θ angle between the X-ray beam and the sample surface), while the integration limits to calculate $I_{sam}(\Delta E)$ and $I_{ref}(\Delta E)$ were set at 288.6 eV and 320 eV.

The comparison between the sp^2 fraction computed from NEXAFS spectra acquired in PEY mode on as-grown, flat a-C:H:Si:O surfaces (equal to 48 ± 2% [31]. Note: the sp^2 fraction obtained from NEXAFS data corrected for the contribution of the contamination layer following the method outline in Ref. [18]) and the fraction of sp^2-bonded carbon calculated on the basis of C K-edge spectra obtained from the STXM transmission analyses of an a-C:H:Si:O lamella (equal to 62 ± 3%) indicated that the preparation of an electron and X-ray transparent lamella does not only lead to variations in local ordering of sp^2 carbon atoms in a-C:H:Si:O, but also to an increase in the fraction of carbon atom in sp^2 hybridization state. This finding is in agreement with previously published studies

highlighting significant variations of the carbon bonding configuration in amorphous carbon materials induced by the exposure to energetic beams (either ions or electrons) [52–54].

The fraction of sp^2 carbon in a-C:H:Si:O could be also computed on the basis of EELS spectra using the same procedure employed for synchrotron-based STXM/NEXAFS measurements (*i.e.*, "NEXAFS method"): the calculated sp^2 fraction, equal to 66 ± 5%, is in close agreement with the results of STXM/NEXAFS analyses (Figure 5).

Owing to its ease of use and flexible energy-loss signal selection, the two-window method (in which the integrated intensity of the π* and σ* orbitals are obtained by integrating the intensity of the C K-edge spectrum over energy windows specific for π* and σ* states, respectively) has also been preferred over functional fitting (in which the π* and σ* absorption features are fitted using synthetic curves, such as Gaussian lines) [55, 56] and model fitting (which relies on background subtraction and integration of the spectra using core excitations) [57, 58] methods to quantify the sp^2 content on the basis of EELS data (see, *e.g.*, [7, 59, 60]). Recently, Zhang *et al.* reviewed the classical two-window method (referred to as "EELS method" in the following) applied to EELS data and suggested optimized settings (*i.e.*, integration limits) for computing the integrated intensities of the π* ($I_{\pi*}$) and σ* ($I_{\sigma*}$) states [33]. The ratio $\frac{I_{\pi*}}{I_{\sigma*}}$ is considered to be proportional to the ratio between the numbers of empty π* and σ* orbitals, which is 1/3 for 100 % sp^2 (*e.g.*, HOPG) and 0/4 for completely sp^3-bond carbon (diamond). In a certain type of carbon material consisting of both sp^2-bond and sp^3-bond carbon, all the π* orbitals contributed by the sp^2-hybridized carbon atoms are accompanied by three σ* orbitals, whereas each sp^3-hybridized C-atom contributes four σ* orbitals. Therefore, for a graphite reference specimen pure in sp^2-C and an unknown C-material containing a fraction of sp^2-hybridized C-atoms the intensity ratios can be written as:

$$\left(\frac{I_{\pi*}}{I_{\sigma*}}\right)_{reference} = k \cdot \frac{1}{3} \qquad\qquad \text{Eq. 2}$$

$$\left(\frac{I_{\pi^*}}{I_{\sigma^*}}\right)_{sample} = k \cdot \frac{x}{4(1-x)+3x} = k \cdot \frac{x}{4-x} \qquad \text{Eq. 3}$$

where k is a pre-factor, which is the partial cross-section ratio between a π^* transition and a σ^* transition, and x is the fraction of sp^2-bonded carbon in the sample ($f_{sp^2(EELS)}$). Equation 2 can be used to remove the dependence on k in Equation 3, and thus the fraction $f_{sp^2(EELS)}$ in the unknown C-material can be expressed as:

$$f_{sp^2(EELS)} = \frac{4\left(\frac{I_{\pi^*}}{I_{\sigma^*}}\right)_{sample} / \left(\frac{I_{\pi^*}}{I_{\sigma^*}}\right)_{reference}}{3+\left(\frac{I_{\pi^*}}{I_{\sigma^*}}\right)_{sample} / \left(\frac{I_{\pi^*}}{I_{\sigma^*}}\right)_{reference}} \qquad \text{Eq. 4}$$

In accordance to previous systematic EELS studies on diamond-like carbon [33], optimized energy integration windows of 284.7-285.3 eV for π^* states and 292-307 eV for σ^* states were chosen for the present EELS quantification. This setting for the π^* states constitutes a compromise between the experimental peak broadening and lifetime broadening of excited states. The narrow integration window largely excludes contributions from C-H bonds, distorted C-bonds with loss signals between the π^* peak and σ^* loss intensities, as well as that from dangling C-bonds below the π^* peak. The fractions of sp^2 carbon atoms in a-C:H:Si:O computed using this approach on the basis of STXM/NEXAFS (equal to 70 ± 3%) and EELS (equal to 69 ± 5%) are still in close agreement (Figure 5). However, the comparison of the quantitative values obtained from the two quantification methodologies (NEXAFS methods *vs.* EELS method) for computing the sp^2 content indicated that, while the results obtained from EELS spectra were not statistically different, a slightly higher amount of carbon atoms in sp^2 hybridization state was calculated from NEXAFS spectra when the quantification is performed using the "EELS method".

It is critical to highlight that the, independently of the method used for the quantification, the results obtained from the STXM/NEXAFS and EELS analysis of a thin a-C:H:Si:O lamella agree well with the fraction of sp^2-bonded carbon atoms computed from NMR measurements (66 ± 5% [37]) (Figure 5). The NMR, EELS, and STXM/NEXAFS, while in all close agreement, are significantly higher than the one

obtained from the NEXAFS spectra acquired in PEY mode on the flat surface of as-grown a-C:H:Si:O films. This result clearly indicates that the destructive preparation of a-C:H:Si:O sample for EELS, STXM/NEXAFS, and NMR analyses induces significant bond breaking and changes in local ordering in the amorphous network of a-C:H:Si:O. This finding highlights the potential influence the sample preparation procedure can have on the structure of metastable materials like amorphous carbons or DLCs.

Conclusions

In summary, a-C:H:Si:O films was characterized by both EELS and transmission STXM/NEXAFS spectroscopy. While the fractions of sp^2-bonded carbon computed using the spectra acquired with these two techniques are in close agreement, the comparison of NEXAFS spectra acquired in transmission STXM mode with NEXAFS spectra acquired in electron yield mode on a flat surface indicated that the destructive preparation of a thin lamella induces variations in the metastable structure of a-C:H:SiO, namely the breakage of carbon-silicon and carbon-hydrogen bonds, a change in local ordering of sp^2-bonded carbon, and an increase in the fraction of sp^2 carbon atoms. These findings can help scientists in the careful interpretation of spectroscopic results obtained from the analysis of samples made of metastable materials after the destructive preparation of specimens for analytical purposes.
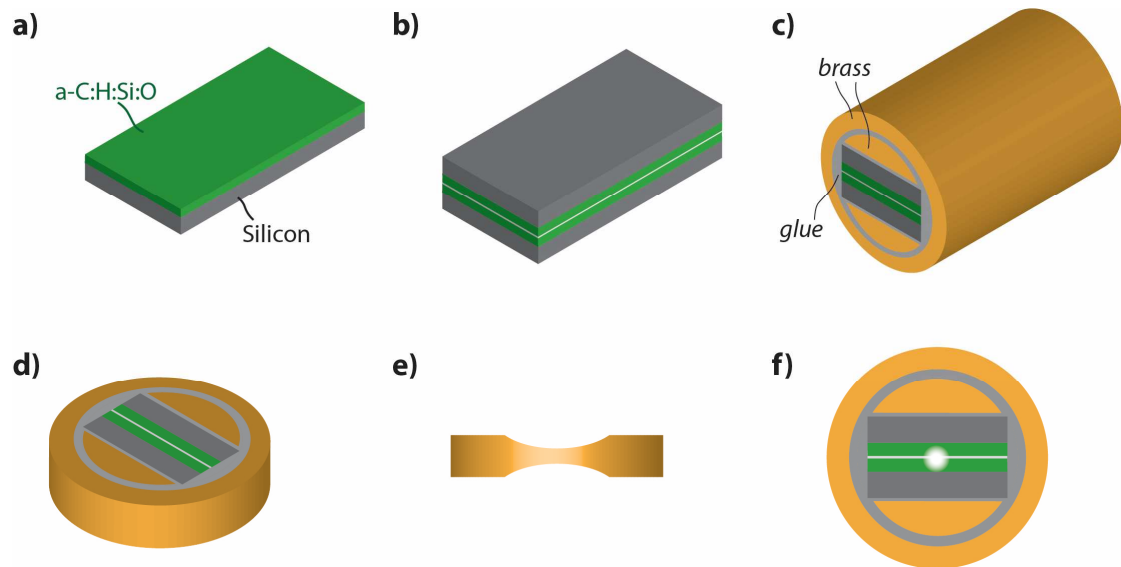
Figures

Figure 1. Schematic for the preparation of a conventional "sandwich" TEM specimen: a) silicon substrate with a-C:H:Si:O coating; b) TEM "sandwich" generated by gluing two a-C:H:Si:O-coated silicon samples against each other (upside/down); c) "sandwich" embedded in a 3-mm-diameter hollow cylinder (prior to this the original sandwich was glued in a full brass cylinder with a slit); d) slice of embedded "sandwich", which is polished down to ~70 µm thickness; e) slice of embedded "sandwich" is dimpled from both sides until the central region is as thin as 2-3 µm; f) further thinning with Ar$^+$ ions using the so-called double-sector technique, which allows for the simultaneous milling of both sides of the lamella in an azimuthally restricted sector that is orthogonal to the central epoxy line of the cross section samples [61], produces a hole in the middle, around which electron-transparent areas suitable for TEM measurements are present. At the final stage, the Ar$^+$ ion energy is reduced to 1 keV to reduce possible sample damage.
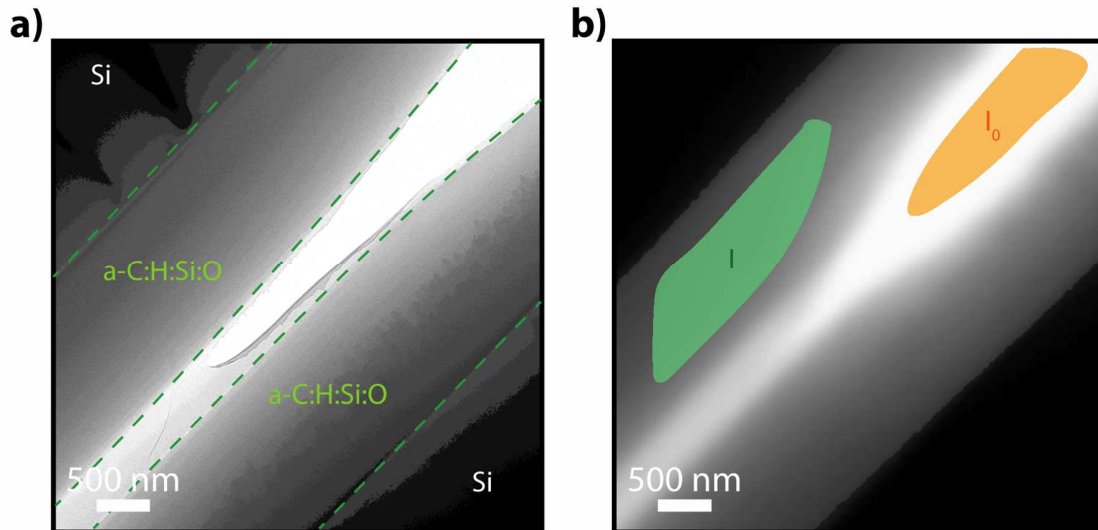
Figure 2. a) Cross-section TEM micrograph of two a-C:H:Si:O-coated silicon samples glued against each other (upside/down); b) average STXM image with regions of interests used for the determination of the intensity of the incoming beam as recorded through a region of the field of view where no sample was present (I_0) and the intensity transmitted through a portion of the sample (I).
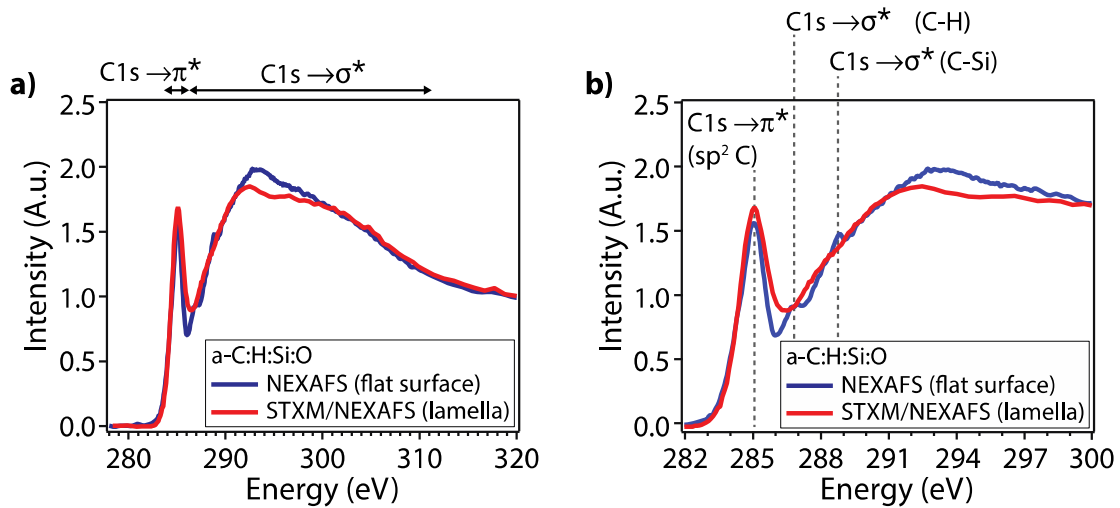
Figure 3. Carbon K-edge NEXAFS spectra ((a) full spectra; (b) zoomed view around the absorption edge) of a-C:H:Si:O acquired in partial electron yield mode ("flat surface" [31]) and in scanning transmission mode ("lamella"). The spectra are pre- and post-edge normalized.
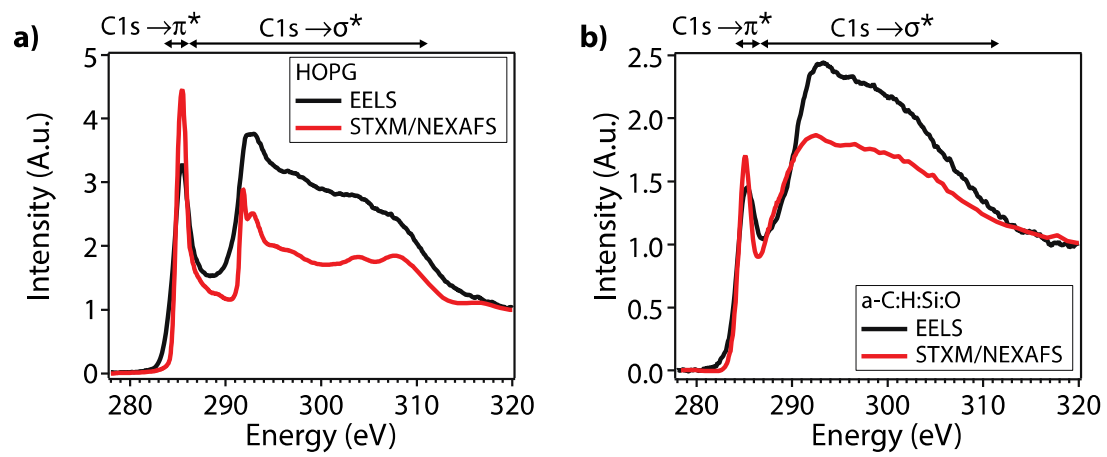
Figure 4. Carbon K-edge NEXAFS spectra of HOPG (a) and a-C:H:Si:O (b). The spectra are pre- and post-edge normalized.
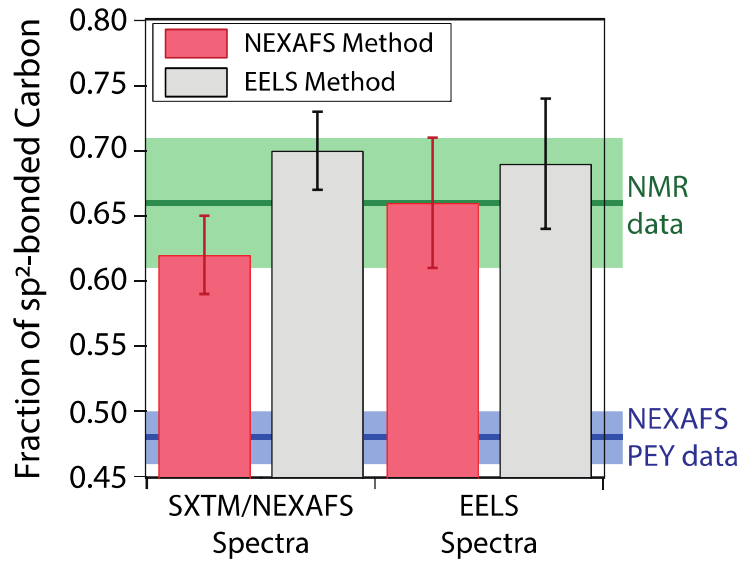
Figure 5. Fraction of sp^2-bonded carbon calculated from SXTM/NEXAFS spectra and EELS spectra using two different methods, namely NEXAFS method (Eq. 1) and EELS method (Eq. 4). For comparison, the sp^2 fraction computed from NEXAFS spectra acquired in PEY mode on as-grown, flat a-C:H:Si:O surfaces (equal to 48 ± 2% [31]) and NMR measurements (66 ± 5% [37]) are reported.

References

1. Robertson, J.: Diamond-like amorphous carbon. Mater. Sci. Eng. R Reports. 37, 129–281 (2002). https://doi.org/10.1016/s0927-796x(02)00005-0

2. Kunze, T., Posselt, M., Gemming, S., Seifert, G., Konicek, A.R., Carpick, R.W., Pastewka, L., Moseler, M.: Wear, plasticity, and rehybridization in tetrahedral amorphous carbon. Tribol. Lett. 53, 119–126 (2014). https://doi.org/10.1007/s11249-013-0250-7

3. Zhang, X., Schneider, R., Müller, E., Mee, M., Meier, S., Gumbsch, P., Gerthsen, D.: Electron microscopic evidence for a tribologically induced phase transformation as the origin of wear in diamond. J. Appl. Phys. 115, 063508 (2014). https://doi.org/10.1063/1.4865742

4. Pastewka, L., Moser, S., Gumbsch, P., Moseler, M.: Anisotropic mechanical amorphization drives wear in diamond. Nat. Mater. 10, (2011). https://doi.org/10.1038/nmat2902

5. Tamor, M.A., Vassell, W.C., Carduner, K.R.: Atomic constraint in hydrogenated "diamond-like" carbon. Appl. Phys. Lett. 58, 592–594 (1991). https://doi.org/10.1063/1.104597

6. Peng, J., Sergiienko, A., Mangolini, F., Stallworth, P.E., Greenbaum, S., Carpick, R.W.: Solid state magnetic resonance investigation of the thermally-induced structural evolution of silicon oxide-doped hydrogenated amorphous carbon. Carbon N. Y. 105, 163–175 (2016). https://doi.org/10.1016/j.carbon.2016.04.021

7. Berger, S.D., McKenzie, D.R., Martin, P.J.: EELS analysis of vacuum arc-deposited diamond-like films. Philos. Mag. Lett. 57, 285–290 (1988). https://doi.org/10.1080/09500838808214715

8. Ponsonnet, L., Donnet, C., Varlot, K., Martin, J.., Grill, A., Patel, V.: EELS analysis of hydrogenated diamond-like carbon films. Thin Solid Films. 319, 97–100 (1998). https://doi.org/10.1016/S0040-6090(97)01094-8

9. Tamor, M.A., Vassell, W.C.: Raman "fingerprinting" of amorphous carbon films. J. Appl. Phys. 76, 3823–3830 (1994). https://doi.org/10.1063/1.357385

10. Ferrari, A.C., Robertson, J.: Interpretation of Raman spectra of disordered and

amorphous carbon. Phys. Rev. B. 61, 14095 (2000).
https://doi.org/10.1007/BF02543692

11. Cui, W.G., Lai, Q.B., Zhang, L., Wang, F.M.: Quantitative measurements of sp3 content in DLC films with Raman spectroscopy. Surf. Coatings Technol. (2010). https://doi.org/10.1016/j.surfcoat.2010.08.093

12. Filik, J., May, P.W., Pearce, S.R.J., Wild, R.K., Hallam, K.R.: XPS and laser Raman analysis of hydrogenated amorphous carbon films. Diam. Relat. Mater. 12, 974–978 (2003). https://doi.org/http://dx.doi.org/10.1016/S0925-9635(02)00374-6

13. Kaciulis, S.: Spectroscopy of carbon: From diamond to nitride films. Surf. Interface Anal. 44, 1155–1161 (2012). https://doi.org/10.1002/sia.4892

14. Diaz, J., Paolicelli, G., Ferrer, S., Comin, F.: Separation of the sp3 and sp2 components in the C1s photoemission spectra of amorphous carbon films. Phys. Rev. B. 54, 8064–8069 (1996)

15. Mangolini, F., Rose, F., Hilbert, J., Carpick, R.W.: Thermally induced evolution of hydrogenated amorphous carbon. Appl. Phys. Lett. 103, 161605 (2013). https://doi.org/doi:http://dx.doi.org/10.1063/1.4826100

16. Mezzi, A., Kaciulis, S.: Surface investigation of carbon films: From diamond to graphite. Surf. Interface Anal. 42, 1082–1084 (2010). https://doi.org/10.1002/sia.3348

17. Lascovich, J.C., Rosato, V.: Analysis of the electronic structure of hydrogenated amorphous carbon via Auger spectroscopy. Appl. Surf. Sci. 152, 10–18 (1999). https://doi.org/10.1016/s0169-4332(99)00310-4

18. Mangolini, F., McClimon, J.B., Rose, F., Carpick, R.W.: Accounting for nanometer-thick adventitious carbon contamination in X-ray absorption spectra of carbon-based materials. Anal Chem. 86, 12258–12265 (2014). https://doi.org/10.1021/ac503409c

19. Kaciulis, S., Mezzi, A., Calvani, P., Trucchi, D.M.: Electron spectroscopy of the main allotropes of carbon. Surf. Interface Anal. 46, 966–969 (2014). https://doi.org/10.1002/sia.5382

20. Lesiak, B., Zemek, J., Jiricek, P., Stobinski, L., Jóźwik, A.: The line shape analysis of electron spectroscopy spectra by the artificial intelligence methods for identification of C sp2/sp3 bonds. Phys. status solidi. 247, 2838–2842 (2010).

https://doi.org/10.1002/pssb.201000245

21. Speranza, G., Laidani, N.: Measurement of the relative abundance of sp2 and sp3 hybridised atoms in carbon based materials by XPS: a critical approach. Part I. Diam. Relat. Mater. 13, 445–450 (2004). https://doi.org/10.1016/j.diamond.2003.11.077

22. Zemek, J., Zalman, J., Luches, A.: XAES and XPS study of amorphous carbon nitride layers. Appl. Surf. Sci. 133, 27–32 (1998). https://doi.org/10.1016/s0169-4332(98)00181-0

23. Mizokawa, Y., Miyasato, T., Nakamura, S., Geib, K.M., Wilmsen, C.W.: Comparison of the CKLL first-derivative auger spectra from XPS and AES using diamond, graphite, SiC and diamond-like-carbon films. Surf. Sci. 182, 431–438 (1987). https://doi.org/10.1016/0039-6028(87)90011-2

24. Mizokawa, Y., Miyasato, T., Nakamura, S., Geib, K.M., Wilmsen, C.W.: The C KLL first-derivative x-ray photoelectron spectroscopy spectra as a fingerprint of the carbon state and the characterization of diamondlike carbon films. J. Vac. Sci. Technol. A Vacuum, Surfaces, Film. 5, 2809–2813 (1987)

25. Lenardi, C., Piseri, P., Briois, V., Bottani, C.E., Bassi, A.L., Milani, P.: Near-edge x-ray absorption fine structure and Raman characterization of amorphous and nanostructured carbon films. J. Appl. Phys. 85, 7159–7167 (1999)

26. Mangolini, F., McClimon, J.B., Carpick, R.W.: Quantitative Evaluation of the Carbon Hybridization State by Near Edge X-ray Absorption Fine Structure Spectroscopy. Anal Chem. 88, 2817–2824 (2016). https://doi.org/10.1021/acs.analchem.5b04525

27. Lenardi, C., Marino, M., Barborini, E., Piseri, P., Milani, P.: Evaluation of hydrogen chemisorption in nanostructured carbon films by near edge X-ray absorption spectroscopy. Eur. Phys. J. B - Condens. Matter Complex Syst. 46, 441–447 (2005). https://doi.org/10.1140/epjb/e2005-00268-2

28. Mangolini, F., Jacobs, T.D.B., Streller, F., McClimon, J.B., Hilbert, J., Lukes, J.R., Carpick, R.W.: Origin of the Thermo-Oxidative Stability of Silicon Oxide-Doped Hydrogenated Amorphous Carbon. (2016)

29. Grierson, D.S., Sumant, A. V, Konicek, A.R., Friedmann, T.A., Sullivan, J.P.,

Carpick, R.W.: Thermal stability and rehybridization of carbon bonding in tetrahedral amorphous carbon. J. Appl. Phys. 107, 33523–33525 (2010)

30. Mangolini, F., McClimon, J.B.: Near Edge X-Ray Absorption Fine Structure Spectroscopy: A Powerful Tool for Investigating the Surface Structure and Chemistry of Solid Lubricants. In: Dienwiebel, M. and De Barros Bouchet, M.I. (eds.) Advanced Analytical Methods in Tribology. pp. 63–106. Springer

31. Mangolini, F., Hilbert, J., McClimon, J.B., Lukes, J.R., Carpick, R.W.: Thermally Induced Structural Evolution of Silicon- and Oxygen-Containing Hydrogenated Amorphous Carbon: A Combined Spectroscopic and Molecular Dynamics Simulation Investigation. Langmuir. 34, 2989–2995 (2018). https://doi.org/10.1021/acs.langmuir.7b04266

32. Mangolini, F., McClimon, J.B., Carpick, R.W.: Quantitative Evaluation of the Carbon Hybridization State by Near Edge X-ray Absorption Fine Structure Spectroscopy. Anal. Chem. acs.analchem.5b04525 (2016). https://doi.org/10.1021/acs.analchem.5b04525

33. Zhang, X., Schneider, R., Müller, E., Gerthsen, D.: Practical aspects of the quantification of sp2-hybridized carbon atoms in diamond-like carbon by electron energy loss spectroscopy. Carbon N. Y. 102, 198–207 (2016). https://doi.org/10.1016/j.carbon.2016.02.020

34. Aarva, A., Deringer, V.L., Sainio, S., Laurila, T., Caro, M.A.: Understanding X-ray Spectroscopy of Carbonaceous Materials by Combining Experiments, Density Functional Theory, and Machine Learning. Part I: Fingerprint Spectra. Chem. Mater. 31, 9243–9255. https://doi.org/10.1021/acs.chemmater.9b02050

35. Aarva, A., Deringer, V.L., Sainio, S., Laurila, T., Caro, M.A.: Understanding X-ray Spectroscopy of Carbonaceous Materials by Combining Experiments, Density Functional Theory, and Machine Learning. Part I: Fingerprint Spectra. Chem. Mater. 31, 9243–9255 (2019). https://doi.org/10.1021/acs.chemmater.9b02049

36. Koshigan, K.D., Mangolini, F., McClimon, J.B., Vacher, B., Bec, S., Carpick, R.W., Fontaine, J.: Understanding the hydrogen and oxygen gas pressure dependence of the tribological properties of silicon oxide–doped hydrogenated amorphous carbon coatings. Carbon N. Y. 93, 851–860 (2015).

https://doi.org/10.1016/j.carbon.2015.06.004

37. Peng, J., Sergiienko, A., Mangolini, F., Stallworth, P.E., Greenbaum, S., Carpick, R.W.: Solid state magnetic resonance investigation of the thermally-induced structural evolution of silicon oxide-doped hydrogenated amorphous carbon. Carbon N. Y. 105, 163–175 (2016). https://doi.org/http://dx.doi.org/10.1016/j.carbon.2016.04.021

38. Mangolini, F., Krick, B.A., Jacobs, T.D.B., Khanal, S.R., Streller, F., McClimon, J.B., Hilbert, J., Prasad, S. V, Scharf, T.W., Ohlhausen, J.A., Lukes, J.R., Sawyer, W.G., Carpick, R.W.: Effect of silicon and oxygen dopants on the stability of hydrogenated amorphous carbon under harsh environmental conditions. Carbon N. Y. 130, 127–136. https://doi.org/10.1016/j.carbon.2017.12.096

39. Hébert, C., Schattschneider, P., Franco, H., Jouffrey, B.: ELNES at magic angle conditions. Ultramicroscopy. 106, 1139–1143 (2006). https://doi.org/10.1016/j.ultramic.2006.04.030

40. Warwick, T., Ade, H., Kilcoyne, D., Kritscher, M., Tylisczcak, T., Fakra, S., Hitchcock, A., Hitchcock, P., Padmore, H.: A new bend-magnet beamline for scanning transmission X-ray microscopy at the Advanced Light Source. J. Synchrotron Radiat. 9, 254–257 (2002). https://doi.org/10.1107/S0909049502005502

41. No Title, http://unicorn.mcmaster.ca/aXis2000.html

42. Mangolini, F., Koshigan, K.D., Van Benthem, M.H., Ohlhausen, J.A., McClimon, J.B., Hilbert, J., Fontaine, J., Carpick, R.W.: How Hydrogen and Oxygen Vapor Affect the Tribochemistry of Silicon- and Oxygen-Containing Hydrogenated Amorphous Carbon: A Study Combining X-Ray Absorption Spectromicroscopy and Data Science Methods. submitted. (2020)

43. Comelli, G., St√∂hr, J., Robinson, C.J., Jark, W.: Structural studies of argon-sputtered amorphous carbon films by means of extended x-ray-absorption fine structure. Phys. Rev. B. 38, 7511–7519 (1988)

44. Sumant, A. V, Gilbert, P.U.P.A., Grierson, D.S., Konicek, A.R., Abrecht, M., Butler, J.E., Feygelson, T., Rotter, S.S., Carpick, R.W.: Surface composition, bonding, and morphology in the nucleation and growth of ultra-thin, high quality nanocrystalline

diamond films. Diam. Relat. Mater. 16, 718–724 (2007). https://doi.org/10.1016/j.diamond.2006.12.011

45. Wada, A., Ogaki, T., Niibe, M., Tagawa, M., Saitoh, H., Kanda, K., Ito, H.: Local structural analysis of a-SiCx:H films formed by decomposition of tetramethylsilane in microwave discharge flow of Ar. Diam. Relat. Mater. 20, 364–367 (2011). https://doi.org/http://dx.doi.org/10.1016/j.diamond.2011.01.020

46. Batson, P.E.: Carbon 1s near-edge-absorption fine structure in graphite. Phys. Rev. B. 48, 2608–2610 (1993)

47. Osswald, S., Yushin, G., Mochalin, V., Kucheyev, S.O., Gogotsi, Y.: Control of sp2/sp3 Carbon Ratio and Surface Chemistry of Nanodiamond Powders by Selective Oxidation in Air. J. Am. Chem. Soc. 128, 11635–11642 (2006). https://doi.org/10.1021/ja063303n

48. Gago, R., Jiménez, I., Albella, J.M., Climent-Font, A., Cáceres, D., Vergara, I., Banks, J.C., Doyle, B.L., Terminello, L.J.: Bonding and hardness in nonhydrogenated carbon films with moderate sp3 content. J. Appl. Phys. 87, 8174–8180 (2000). https://doi.org/doi:http://dx.doi.org/10.1063/1.373514

49. Gago, R., Jiménez, I., Albella, J.M.: Detecting with X-ray absorption spectroscopy the modifications of the bonding structure of graphitic carbon by amorphisation, hydrogenation and nitrogenation. Surf. Sci. 482–485, P, 530–536 (2001). https://doi.org/http://dx.doi.org/10.1016/S0039-6028(01)00939-6

50. Konicek, A.R., Grierson, D.S., Gilbert, P.U.P.A., Sawyer, W.G., Sumant, A. V, Carpick, R.W.C.N.-6: Origin of Ultralow Friction and Wear in Ultrananocrystalline Diamond. Phys. Rev. Lett. 100, 235502 (2008)

51. Sumant, A.V., Grierson, D.S., Gerbi, J.E., Birrell, J., Lanke, U.D., Auciello, O., Carlisle, J.A., Carpick, R.W.: Toward the Ultimate Tribological Interface: Surface Chemistry and Nanotribology of Ultrananocrystalline Diamond. Adv. Mater. 17, 1039–1045 (2005). https://doi.org/10.1002/adma.200401264

52. Francz, G., Reinke, P., Oelhafen, P., Hänni, W.: Photoelectron spectroscopy of ion-irradiated B-doped CVD diamond surfaces. Thin Solid Films. 270, 200–204 (1995). https://doi.org/10.1016/0040-6090(95)06916-x

53. Caro, M.A., Deringer, V.L., Koskinen, J., Laurila, T., Csanyi, G.: Growth

Mechanism and Origin of High sp^{3} Content in Tetrahedral Amorphous Carbon. Phys Rev Lett. 120, 166101 (2018). https://doi.org/10.1103/PhysRevLett.120.166101

54. Zemek, J., Jiricek, P., Houdkova, J., Artemenko, A., Jelinek, M.: Diamond-like carbon and nanocrystalline diamond film surfaces sputtered by argon cluster ion beams. Diam. Relat. Mater. 68, 37–41 (2016). https://doi.org/10.1016/j.diamond.2016.06.003

55. Silvaf, S.R.P., Robertson, J., Rusli, Amaratunga, G.A.J., Schwan, J.: Structure and luminescence properties of an amorphous hydrogenated carbon. Philos. Mag. Part B. 74, 369–386 (1996). https://doi.org/10.1080/01418639608240341

56. Bernier, N., Bocquet, F., Allouche, A., Saikaly, W., Brosset, C., Thibault, J., Charaï, A.: A methodology to optimize the quantification of sp2 carbon fraction from K edge EELS spectra. J. Electron Spectros. Relat. Phenomena. 164, 34–43 (2008). https://doi.org/http://dx.doi.org/10.1016/j.elspec.2008.04.006

57. Titantah, J.T., Lamoen, D.: Technique for the sp2/sp3 characterization of carbon materials: Ab initio calculation of near-edge structure in electron-energy-loss spectra. Phys. Rev. B - Condens. Matter Mater. Phys. 70, 075115 (2004). https://doi.org/10.1103/PhysRevB.70.075115

58. Verbeeck, J., Bertoni, G.: Model-based quantification of EELS: Is standardless quantification possible? In: Microchimica Acta. pp. 439–443. Springer (2008)

59. BRULEY, J., WILLIAMS, D.B., CUOMO, J.J., PAPPAS, D.P.: Quantitative near-edge structure analysis of diamond-like carbon in the electron microscope using a two-window method. J. Microsc. 180, 22–32 (1995). https://doi.org/10.1111/j.1365-2818.1995.tb03653.x

60. Cuomo, J.J., Doyle, J.P., Bruley, J., Liu, J.C.: Sputter deposition of dense diamond-like carbon films at low temperature. Appl. Phys. Lett. 58, 466–468 (1991). https://doi.org/doi:http://dx.doi.org/10.1063/1.104609

61. Dieterle, L., Butz, B., Muller, E.: Optimized Ar(+)-ion milling procedure for TEM cross-section sample preparation. Ultramicroscopy. 111, 1636–1644 (2011). https://doi.org/10.1016/j.ultramic.2011.08.014

Electron energy -loss spectrometers (EELS) and **Scanning Transmission X-ray Microscopy (SXTM)**

a-C:H:Si:O

Detector

Silicon

Impinging electron beam or **X-ray photons**

a-C:H:Si:O
— EELS
— STXM/NEXAFS